

## Article

# Characterization of an Amazon Soil Profile by Laser-Induced Breakdown, Raman, and Fluorescence Spectroscopies

José L. Clabel Huamán <sup>1</sup>, Amanda Maria Tadini <sup>2</sup>, Giorgio Saverio Senesi <sup>3</sup> , Stéphane Mounier <sup>2</sup> , Débora M. B. P. Milori <sup>4</sup> and Gustavo Nicolodelli <sup>5,\*</sup> 

<sup>1</sup> São Carlos Institute of Physics, University of São Paulo, Sao Carlos 13566-590, Brazil

<sup>2</sup> Mediterranean Institute of Oceanology, University of Toulon, 83130 Toulon, France

<sup>3</sup> CNR—Istituto per la Scienza e Tecnologia dei Plasmi (ISTP), Bari Seat, 70126 Bari, Italy

<sup>4</sup> Embrapa Instrumentation, Sao Carlos 13560-970, Brazil

<sup>5</sup> Department of Physics, Federal University of Santa Catarina, Florianópolis 88040-900, Brazil

\* Correspondence: gustavo.nicolodelli@ufsc.br

**Abstract:** This work aimed to investigate, in detail, the elemental and molecular composition of soil samples collected from the various horizons of an Amazon spodosol profile by combining the atomic technique laser-induced breakdown spectroscopy (LIBS) with two molecular techniques, i.e., Raman and fluorescence spectroscopies. The emission lines of the elements Fe, C, Si, Mg, Al, Ti, Ca, and K with various relative intensities were detected by using LIBS. In particular, C appeared to accumulate in the transition horizon and was proven to be mostly humified by fluorescence analysis. The Raman peaks detected at 465 cm<sup>-1</sup> and 800 cm<sup>-1</sup> corresponded with the symmetric stretching and bending modes of O-Si-O and Si-OH, respectively. Small shifts toward higher frequencies and slight increases in the width and full width at half maximum (FWHM) of the quartz band at 465 cm<sup>-1</sup> appeared in the Tr to K2 horizons, which could be ascribed to a local distortion caused by the high contents of Al of kaolinite mineral phases, as also shown by the LIBS data. Thus, a small amount of kaolinite mineral phase and K measured by LIBS would be present also in the A1 to E2 horizons. The lifetime fluorescence was almost constant in the surface and middle horizons, whereas it increased sharply in the transition horizon and then decreased slightly in the kaolin horizons, which confirmed the presence of more humified recalcitrant organic matter in deeper soil horizons. In conclusion, the combined use of the three spectroscopic techniques appeared to be a very promising approach for studying Amazon soils.

**Keywords:** Amazon soils; laser-induced breakdown spectroscopy; Raman spectroscopy; fluorescence spectroscopy



**Citation:** Huamán, J.L.C.; Tadini, A.M.; Senesi, G.S.; Mounier, S.; Milori, D.M.B.P.; Nicolodelli, G.

Characterization of an Amazon Soil Profile by Laser-Induced Breakdown, Raman, and Fluorescence

Spectroscopies. *Minerals* **2023**, *13*, 553. <https://doi.org/10.3390/min13040553>

Academic Editor: Hongfei Cheng

Received: 6 March 2023

Revised: 5 April 2023

Accepted: 10 April 2023

Published: 14 April 2023



**Copyright:** © 2023 by the authors. Licensee MDPI, Basel, Switzerland. This article is an open access article distributed under the terms and conditions of the Creative Commons Attribution (CC BY) license (<https://creativecommons.org/licenses/by/4.0/>).

## 1. Introduction

The Amazon rainforest features a very rich and complex biome of relevant global importance and is considered to be one of the most important and highly susceptible to climate change carbon sinks on Earth [1,2]. The spodosols below the Amazon rainforest are typically accumulating a great quantity of soil organic matter (SOM) on their surface and along their profile [3–5]; thus, a more extended study of them is extremely important. Laser-induced breakdown spectroscopy (LIBS) is a very versatile technique widely applied in several research areas, including the environmental sector, and offers the possibility of on-site measurements [6–10]. In particular, this technology can rapidly and accurately detect and identify the constituent chemical elements, i.e., provide a “chemical fingerprint” of the analyzed material, thus allowing the characterization of diverse organic and inorganic materials in real-time, requiring no sample preparation and offering high sensitivity and specificity [11]. Additionally, Raman spectroscopy is a powerful, non-destructive consolidated technique for molecular analysis [12] and is widely applied to various types of agro-environmental samples [13–15], also featuring a possible use for in situ analysis.

Finally, fluorescence spectroscopy is a very sensitive technique widely applied for the selective study of “fluorophores” and to investigate the processes of interaction between metal ions and organic matter in soils, providing specific analysis of the structure and dynamics of macromolecules [5,6,16–19].

The objective of this work was to combine the three complementary spectroscopy techniques mentioned above as a very attractive approach for an Amazon soil profile characterization.

## 2. Materials and Methods

### 2.1. Soil Samples

Soil samples were collected from a humiluvic spodosol profile located on the northern shore of the Rio Negro River near the city of São Gabriel da Cachoeira (0°6′24.5″ S; 66°54′19.3″ W), Amazonas State, Brazil. In particular, soils were sampled from nine horizons, i.e., superficial (A1, A2), albic (E1, E2), spodic (Bh, Bhs), transition (Tr), and kaolin (K1, K2). Soil samples were oven-dried at 35 °C, and after, they were sieved at 2 mm to remove the roots, then they were crushed and sieved to <0.250 mm (60 mesh). For the analyses, the soil samples were pelletized (1 cm × 2 mm at approximately 0.5 g) with a hydraulic press. Detailed descriptions of these horizons and their mineralogical and chemical data can be found in [4,19,20].

### 2.2. Laser-Induced Breakdown Spectroscopy

The LIBS system consisted of an Nd: YAG laser operating at 1064 nm and an ARYELLE 400-Butterfly spectrometer as a detection system. The spectrometer operated in two spectral bands of 175–340 nm and 275–770 nm, with spectral resolutions of 13–24 pm and 29–80 pm, respectively, equipped with an intensified charge-coupled device (ICCD) camera with 1024 × 1024 pixels. Two lenses (telescope assembly) were placed between the sample and the input of the fiber to increase the light collected from the plasma. A xy scanning stage was used to control the target positions on the sample. An eight-channel pulse generator (Model 9618, Quantum Composers, Bozeman, MT, USA) was used to synchronize the delay time between the laser pulse and acquisition during the measurements. The LIBS spectra were acquired using 5-pulse accumulation at each target position, with each pulse having an energy of 75 mJ and a width of 6 ns in a 5 mm diameter beam focused by a 100 mm lens. An optimal distance lens to sample was fixed at about 100 mm, which assured the lowest standard deviation in measurements between successive sampling spots. The delay time of detection and the ICCD gate width were set at 1 μs and 10 μs, respectively. A total of 10 spectra were acquired for each sample.

### 2.3. Raman Spectroscopy

The Raman spectra were measured on pellets of whole soil samples at room temperature using a Raman spectrometer (RAM II Bruker) provided with an excitation source of 1064 nm that operates up to a power of 500 mW and features a spectral resolution of 2 cm<sup>-1</sup>. The spectra were acquired from a scan number of 32 and a power of 100 mW. Twelve spectra were acquired from each sample at 80 to 1300 cm<sup>-1</sup>. Then, the experimental spectra were fitted to a Lorentzian peak profile and a second-order polynomial for the background correction. The average Raman spectrum of each sample was compared with the RRUFF database to identify each horizon’s mineral phase.

### 2.4. Fluorescence Spectroscopy and Fluorescence Lifetime

The steady-state fluorescence emission spectra at the excitation of 485 nm were recorded by a FluoTime 300 Instrument (PicoQuant, Berlin, Germany) equipped with a pico sec-pulsed laser diode LDH-P-C-405 and a detector H01033-45 (Hamamatsu, Japan). The fluorescence lifetime was recorded using the time-correlated single photon counting (TCSPC) method at the emission and excitation wavelengths of 548 nm and 405 nm, respectively. The lifetime was then analyzed by the PicoQuant FluoFit4 program that uses a multi-exponential fitting model:  $I(t) = \sum_i \alpha_i e^{-t/\tau_i}$ , where  $\alpha_i$  is the fractional amplitude of

the intensity decay of the  $i$ th component at time  $t$ , and  $\tau_i$  is the lifetime of the  $i$ th component. The amplitude ( $\langle\tau\rangle_{amp}$ ) and the intensity-weighted ( $\langle\tau\rangle_{int}$ ) average lifetime were calculated using the following expressions:  $\langle\tau\rangle_{amp} = \frac{\sum_i \alpha_i \tau_i}{\sum_i \alpha_i}$  and  $\langle\tau\rangle_{int} = \sum_i f_i \tau_i$ , where  $f_i$  represents the fractional intensities of each fluorescence lifetime component.

### 3. Results and Discussion

#### 3.1. LIBS Spectra

The emission lines of the elements C (247.86 nm), Fe (259.940 nm), Mg (279.55, 280.27, and 285.213 nm), Si (288.16 nm), Al (308 and 394.40 nm), Ti (375.93 nm), Ca (393.36 and 422.67 nm), and K (766.49 and 769.90 nm) were identified in the LIBS spectra of soils from the various horizons (Figure 1 and Figure S1—Supplementary Materials) and are reported in Table 1, and their relative emission intensities (in arbitrary units, a.u.) are shown Figure 2.

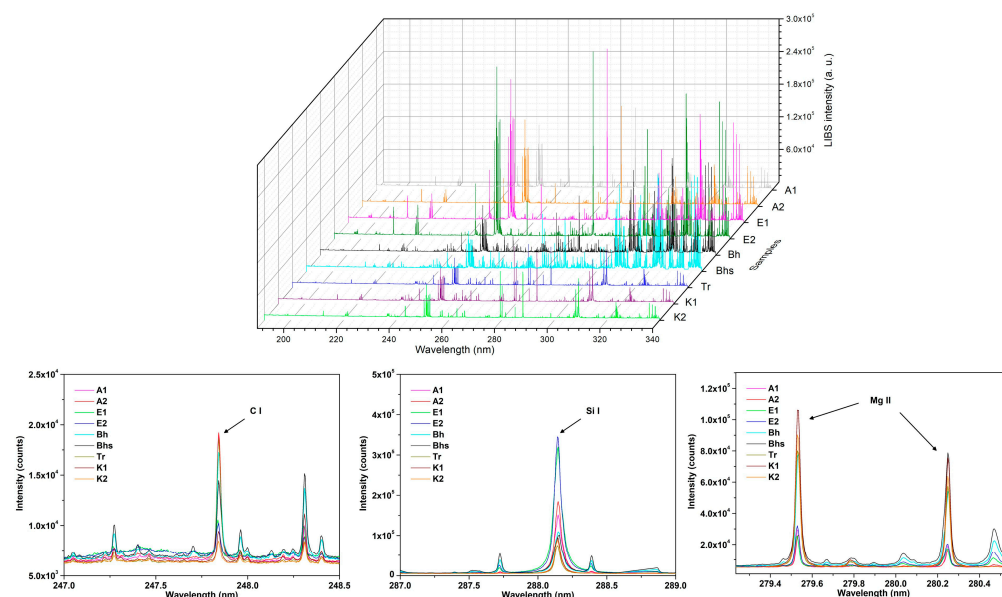


**Figure 1.** Average LIBS spectra in the UV region of soil samples from all horizons. Additionally, an enlarged region of three emission peaks was analyzed.

**Table 1.** Main emission lines of the elements identified in the LIBS spectra of soils from the various horizons.

Emission Lines	Wavelength (nm)
C I	247.86
Mg II	279.55; 280.27
Mg I	285.21
Fe II	238.20; 239.56; 259.94; 274.91; 275.57
Si I	288.16
Al I	308.21; 394.40
Ti II	375.93
Ca I	393.36
Ca II	422.67
K I	766.49; 769.90

The relative emission intensity of the Fe line varied along the profile with evidence of accumulation in the Bh and Bhs horizons, which confirms that the accumulation of this element may be associated with the formation process of these types of spodosols [6]. As expected, the C emission line showed the highest relative intensity in soils from the surface horizon (A1 and A2), with a tendency to decrease and then accumulate again in the Bh and Tr horizons [4,21,22]. Differently, the Si emission line intensity was the highest in the E horizons, whereas the intensity of the Mg and Al emission lines appeared to follow a similar

trend along the profile with the highest values for soils from deeper horizons where clay predominates [4]. The Ti emission line intensity was the highest in the Bh and E horizons, which suggests the large presence of titanium oxide in these horizons [4]. Additionally, the emission line intensity of Ca was the highest in the Bh horizons, whereas the highest intensity of the K lines was featured in the Bh and Bhs horizons and the K horizons, which may be attributed to the presence of large amounts of quartz, kaolinite, and anatase [4].

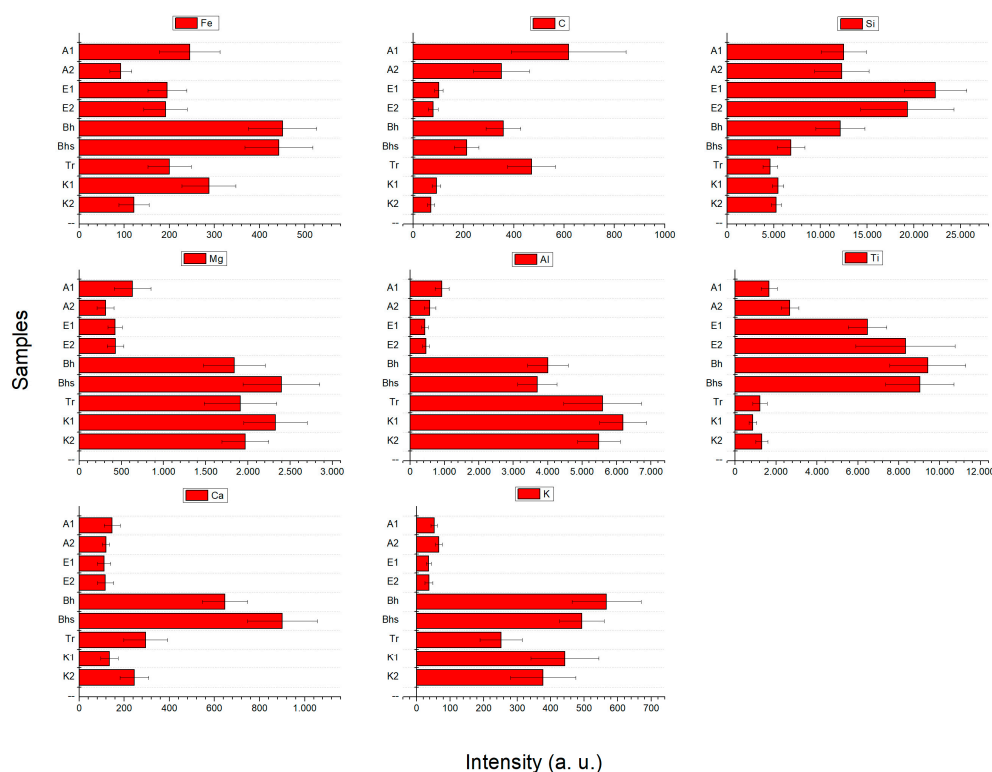


**Figure 2.** Relative emission line intensities (in arbitrary units, a.u.) of the elements Fe, C, Mg, Si, Al, Ti, Ca, and K in LIBS spectra of soil samples from different horizons.

### 3.2. Raman Spectra

The Raman spectra measured for soils from the various horizons are shown in Figure 3a, whereas the Raman shift and full width at half maximum (FWHM) of some relevant bands are reported in Figure 3b,c. In particular, the characteristic Raman bands of quartz were observed at about 207, 465, and 800  $\text{cm}^{-1}$ . The position and peak intensity of the weak band around 207  $\text{cm}^{-1}$ , likely due to the O-Si-O bond influenced by Al substitution in the various horizons, varied depending on the clay mineral type, whereas the peaks at 465  $\text{cm}^{-1}$  and 800  $\text{cm}^{-1}$  correspond to the symmetric stretching bending modes of O-Si-O and Si-OH. The two peaks of various intensities at  $\sim 128 \text{ cm}^{-1}$  and  $\sim 147 \text{ cm}^{-1}$  could be assigned to the O-Al-O and O-Si-O symmetric bends of kaolinite, respectively. Thus, besides the Bh and Bhs horizons, a small amount of kaolinite mineral phase could also be measured by Raman spectroscopy in the A1 to E2 horizons, where it could not be detected by X-ray diffraction because it was below the detection limit. However, as previously reported, weak sharp peaks at about 3696, 3668, 3653, and 3620  $\text{cm}^{-1}$  corresponding to the O-H group that coordinates with  $\text{Al}^{3+}$  in the octahedral sites ( $\text{Al}(\text{OH})_3$ ) of the kaolinite structure were confirmed by FTIR [22,23]. Moreover, small planar particles on the particle surface of the A1 horizon are attributed to a kaolinite phase identified by the SAED pattern [4].

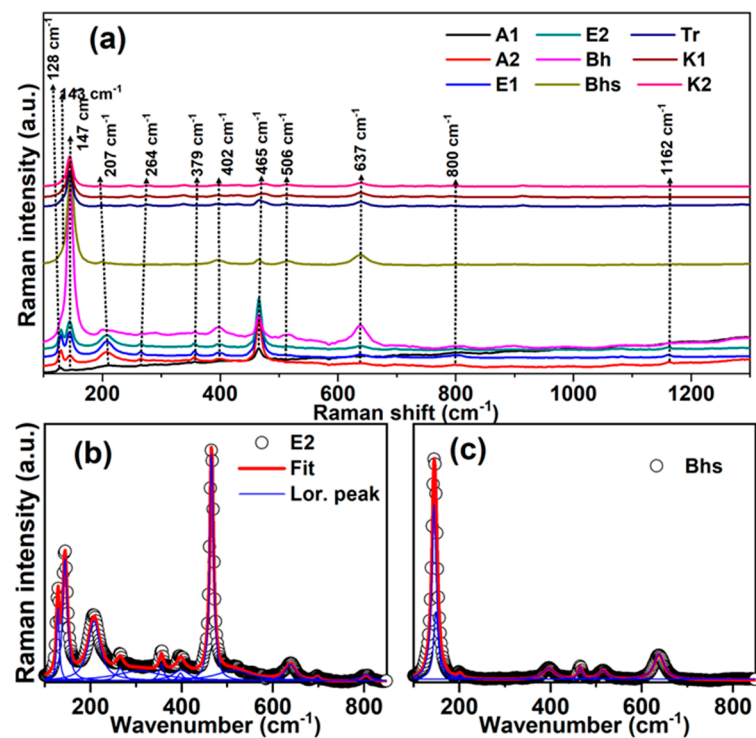


**Figure 3.** (a) Raman spectra of the humiluvic spodosol profile. Deconvoluted spectra resolved from curve fitting and fitted spectrum to the layers in (b) E2 and (c) Bhs.

Noteworthy, the shoulder at  $143\text{ cm}^{-1}$  of the intense band at  $\sim 147\text{ cm}^{-1}$  and the peak at  $637\text{ cm}^{-1}$  identified in the spectra of samples from the Bh and Bhs horizons could be attributed to the presence of anatase. In particular, the overlapping of adjacent peaks around  $147\text{ cm}^{-1}$  might be ascribed to the presence of quartz, kaolinite, and anatase mineral phases in the Bh and Bhs horizons. Furthermore, the weak peaks at  $\sim 264$ ,  $\sim 379$ ,  $\sim 402$ , and  $\sim 506\text{ cm}^{-1}$  due to Al-O-Al deformation and Al-O stretching vibrations, which are, in some cases, overlapped by kaolinite peaks, could be attributed to the gibbsite mineral phase.

To gain more information on the observed spectral modifications, i.e., the Raman shift and FWHM, a deconvoluted spectrum resolved from curve fitting and fitted spectrum to the layers E2 (Figure 3b) and Bhs (Figure 3c) was performed using the Lorentzian function. The deconvoluted spectra resolved from curve fitting and fitted spectrum to the layers and the detected peaks identified are shown in the Supplementary Materials (Figure S2 and Table S1). In particular, the peak position and FWHM at  $128$  and  $147\text{ cm}^{-1}$  appeared displaced significantly in the transition from the E2 to Bh profile (Figure 3b), which might be due to significant chemical variations in quartz, kaolinite, and other minerals, such as anatase, and/or to different organic matter content (as revealed by the LIBS spectra) [24,25]. Differently from FWHM, no significant change was apparent for the peak of anatase at  $637\text{ cm}^{-1}$ , as can be observed in Table S1A (see Supplementary Materials), which might be related to the crystalline size of anatase particles and the presence of defects or impurities in the anatase lattice that may cause lattice strain and, thus, broaden the peaks [26]. No pronounced changes were apparent for the position and FWHM of the quartz band at  $465\text{ cm}^{-1}$  passing from the A1 to Bhs horizon, as can be seen in Table S1A (see Supplementary Materials). Although the entire profile is rich in quartz mineral phase, as shown by the LIBS intense peak of Si (Figure 2), small shifts toward higher frequencies and slight increases in the width and FWHM of the quartz band at  $465\text{ cm}^{-1}$  were apparent passing from the Tr to the K2 horizon (see Supporting Information). These shifts might be correlated with a local distortion caused by the high Al content of the kaolinite mineral phase [27,28], as confirmed by the LIBS data (Figure 2) and XRD measurements in the Supplementary Materials (Figure S3) [4].

### 3.3. Fluorescence Spectra and Lifetime Analysis

The fluorescence spectra ( $\lambda_{exc} = 485 \text{ nm}$ ) (Figure 4a) of soils from various horizons featured a typical wide band with a maximum intensity at about 540–560 nm [5,29]. The shift from shorter to longer wavelengths that occurred passing from the K1 to Tr horizons suggests the increasing presence of more extensively humified SOM [5]. The deconvolution of the spectra (Figure 4b) yielded four peaks, all at a wavelength higher than 530 nm, which could be associated with the presence of four fluorophores that would suggest an extended humification level of SOM [30], especially in the deeper Tr and K horizons.

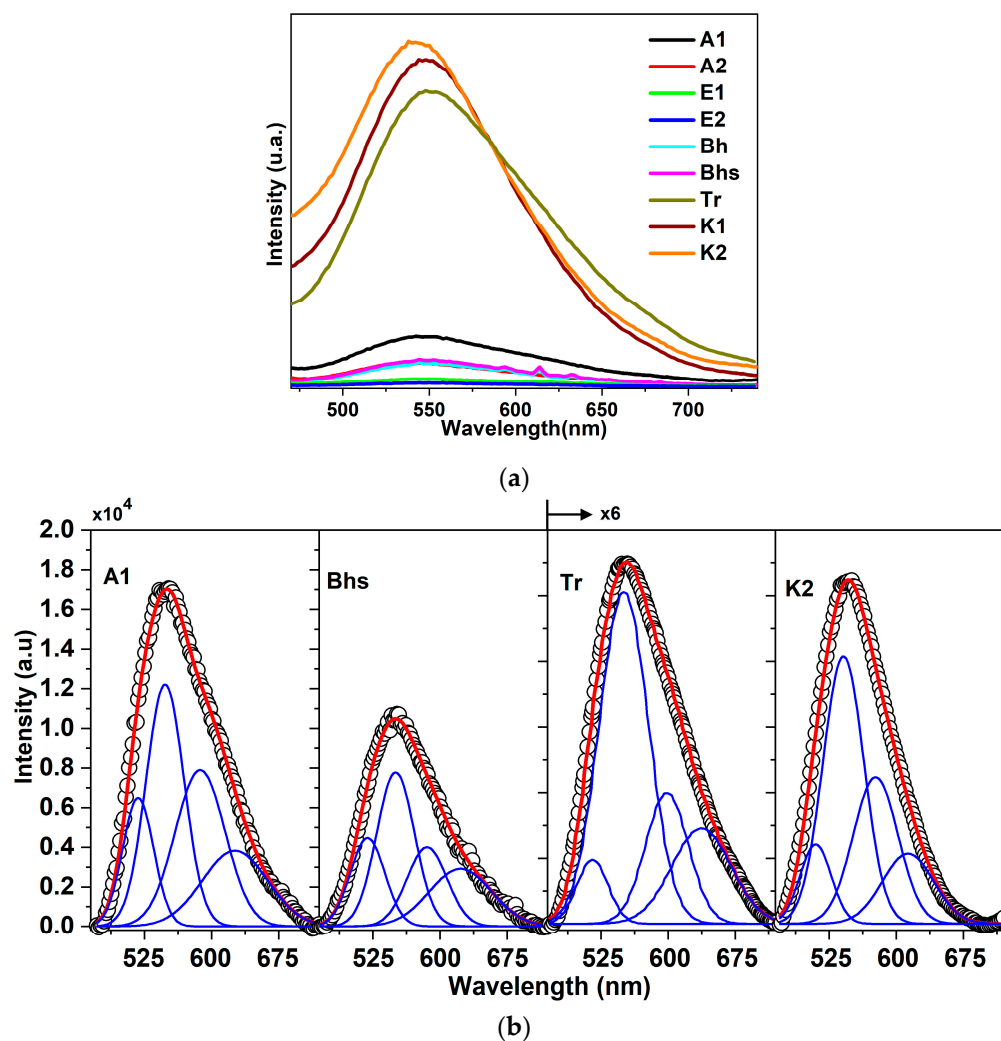


**Figure 4.** Fluorescence emission spectra were measured at an excitation of 485 nm on soils from the various horizons (a) and the corresponding deconvoluted spectra of soils from A1, Bhs, Tr, and K2 horizons (b).

The fluorescence lifetime, measured as fluorescence intensity in a.u. (Figure 5), was almost constant for soils from the A, E, and Bhs horizons, then it showed a sharp increase in the Tr soil and decreased slightly in K soils. This trend confirms the emission fluorescence data in suggesting the presence in the deeper horizons of more reactive and structurally complex, i.e., more extensively humified, SOM, which could influence, markedly, metal mobility and availability [5]. These data, besides confirming previous findings, i.e., that the humification index of SOM increased especially in the Tr, K1, and K2 horizons [19], also suggest that SOM rich in aromatic condensed rings, i.e., the most extensively humified SOM, was transferred from the Bh horizons and accumulated in the Tr and K horizons.

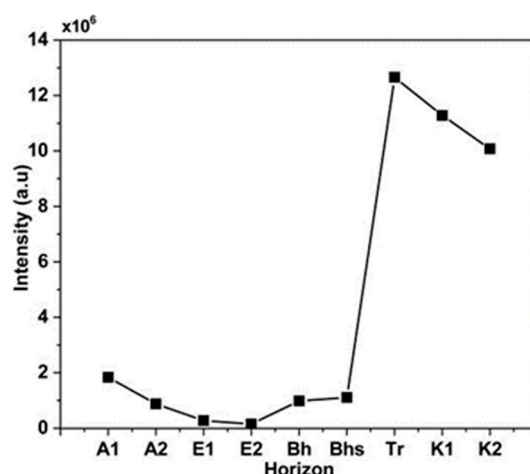


**Figure 5.** Fluorescence lifetime at an excitation of 410 nm of soils from the various horizons.

#### 4. Conclusions

This study showed, for the first time, that the combination of LIBS, Raman, and fluorescence spectroscopies can be used successfully to investigate the elemental and molecular composition of the various soil horizons along an Amazon spodosol profile. In particular, the three techniques were shown to complement each other, as LIBS can provide detailed information on the multi-elemental composition of the sample, while Raman and fluorescence spectroscopies can yield information on the molecular aspects. This approach allowed us to evaluate the composition of soils of the various horizons and correlate qualitatively this information with soil mineralogy along the various horizons. Furthermore, fluorescence data revealed the presence of a more reactive, extensively humified SOM in the Tr and K horizons, which may influence, markedly, the mobility and availability of metals in the soil profile. In conclusion, the three spectroscopic techniques used display several characteristics that, when combined, provide a very attractive approach to the characterization of soils.

**Supplementary Materials:** The following supporting information can be downloaded at: <https://www.mdpi.com/article/10.3390/min13040553/s1>, Figure S1: Average LIBS spectra in the VIS region of soil samples from all horizons, Figure S2: Deconvoluted spectra resolved from curve-fitting and fitted spectrum from different layers, Figure S3: Rietveld refinement of their XRPD patterns. SO quartz, KO kaolinite, Gb gibbsite, TO titanium oxide (anatase), MO muscovite. (Adapted from Huaman [4]). Copyright 2021, with permission from Springer, Table S1. Raman wavenumbers ( $\text{cm}^{-1}$ ) were observed for quartz (SO), kaolinite (KO), gibbsite (Gb), anatase (TO), and muscovite (MO) from different layers.

**Author Contributions:** Conceptualization, J.L.C.H., A.M.T. and G.N.; methodology, J.L.C.H., S.M. and G.N.; validation, J.L.C.H., G.S.S. and G.N.; formal analysis, J.L.C.H., A.M.T., G.S.S., S.M. and G.N.; investigation, J.L.C.H. and G.N.; resources, D.M.B.P.M.; writing—original draft preparation, J.L.C.H. and G.N.; writing—review and editing, J.L.C.H., A.M.T., G.S.S., D.M.B.P.M. and G.N.; supervision, D.M.B.P.M. and G.N.; project administration, D.M.B.P.M.; funding acquisition, D.M.B.P.M. and G.N. All authors have read and agreed to the published version of the manuscript.

**Funding:** This work was partially supported by Conselho Nacional de Desenvolvimento Científico e Tecnológico—CNPq (grant number: 313685/2020-7).

**Data Availability Statement:** Not applicable.

**Conflicts of Interest:** The authors declare no conflict of interest.

## References

1. Denning, S. Southeast Amazonia Is No Longer a Carbon Sink. *Nature* **2021**, *595*, 354–355. [[CrossRef](#)] [[PubMed](#)]
2. Gatti, L.v.; Basso, L.S.; Miller, J.B.; Gloor, M.; Gatti Domingues, L.; Cassol, H.L.G.; Tejada, G.; Aragão, L.E.O.C.; Nobre, C.; Peters, W.; et al. Amazonia as a Carbon Source Linked to Deforestation and Climate Change. *Nature* **2021**, *595*, 388–393. [[CrossRef](#)] [[PubMed](#)]
3. Montes, C.R.; Lucas, Y.; Pereira, O.J.R.; Achard, R.; Grimaldi, M.; Melfi, A.J. Deep Plant-Derived Carbon Storage in Amazonian Podzols. *Biogeosciences* **2011**, *8*, 113–120. [[CrossRef](#)]
4. Clabel Huamán, J.L.; Nicolodelli, G.; Senesi, G.S.; Montes, C.R.; Felicio Perruci, N.A.; Bezzon, V.D.N.; Milori, D.M.B.P. Characterization and Distribution of Mineral Phases in an Amazonian Humiluvic Spodosol Profile by XRPD, HR-TEM, SAED and SEM–EDX. *Environ. Earth Sci.* **2021**, *80*, 405. [[CrossRef](#)]
5. Tadini, A.M.; Nicolodelli, G.; Hajjoul, H.; Milori, D.M.B.P.; Mounier, S. Humic Fractions from Amazon Soils: Lifetime Study and Humification Process by Fluorescence Spectroscopy. *Appl. Geochem.* **2022**, *147*, 105486. [[CrossRef](#)]
6. Tadini, A.M.; Nicolodelli, G.; Marangoni, B.S.; Mounier, S.; Montes, C.R.; Milori, D.M.B.P. Evaluation of the Roles of Metals and Humic Fractions in the Podzolization of Soils from the Amazon Region Using Two Analytical Spectroscopy Techniques. *Microchem. J.* **2019**, *144*, 454–460. [[CrossRef](#)]
7. Gonçalves, D.A.; Senesi, G.S.; Nicolodelli, G. Laser-Induced Breakdown Spectroscopy Applied to Environmental Systems and Their Potential Contaminants. An Overview of Advances Achieved in the Last Few Years. *Trends Environ. Anal. Chem.* **2021**, *30*, e00121. [[CrossRef](#)]
8. Nicolodelli, G.; Cabral, J.; Menegatti, C.R.; Marangoni, B.; Senesi, G.S. Recent Advances and Future Trends in LIBS Applications to Agricultural Materials and Their Food Derivatives: An Overview of Developments in the Last Decade (2010–2019). Part I. Soils and Fertilizers. *TrAC Trends Anal. Chem.* **2019**, *115*, 70–82. [[CrossRef](#)]
9. Krüger, A.L.; Nicolodelli, G.; Villas-Boas, P.R.; Watanabe, A.; Milori, D.M.B.P. Quantitative Multi-Element Analysis in Soil Using 532 Nm and 1064 Nm Lasers in LIBS Technique. *Plasma Chem. Plasma Process.* **2020**, *40*, 1417–1427. [[CrossRef](#)]
10. de Moraes, C.P.; Nicolodelli, G.; Mitsuyuki, M.C.; Mounier, S.; Milori, D.M.B.P. Optimization of Laser-Induced Breakdown Spectroscopy Parameters from the Design of Experiments for Multi-Element Qualitative Analysis in River Sediment. *Spectrochim. Acta Part B Spectrosc.* **2021**, *177*, 106066. [[CrossRef](#)]
11. Hahn, D.W.; Omenetto, N. Laser-Induced Breakdown Spectroscopy (LIBS), Part I: Review of Basic Diagnostics and Plasma—Particle Interactions: Still-Challenging Issues within the Analytical Plasma Community. *Appl. Spectrosc.* **2010**, *64*, 335A–336A. [[CrossRef](#)] [[PubMed](#)]
12. Yeturu, S.; Vargas Jentsch, P.; Ciobotă, V.; Guerrero, R.; Garrido, P.; Ramos, L.A. Handheld Raman Spectroscopy for the Early Detection of Plant Diseases: Abutilon Mosaic Virus Infecting Abutilon sp. *Anal. Methods* **2016**, *8*, 3450–3457. [[CrossRef](#)]
13. Xing, Z.; Du, C.; Zeng, Y.; Ma, F.; Zhou, J. Characterizing Typical Farmland Soils in China Using Raman Spectroscopy. *Geoderma* **2016**, *268*, 147–155. [[CrossRef](#)]
14. Xing, Z.; Du, C.; Tian, K.; Ma, F.; Shen, Y.; Zhou, J. Application of FTIR-PAS and Raman Spectroscopies for the Determination of Organic Matter in Farmland Soils. *Talanta* **2016**, *158*, 262–269. [[CrossRef](#)] [[PubMed](#)]
15. Giannetta, B.; Cassetta, M.; Oliveira de Souza, D.; Mariotto, G.; Aquilanti, G.; Zaccone, C. Coupling X-Ray Absorption and Raman Spectroscopies to Characterize Iron Species in a Karst Pedosedimentary Record. *Soil Syst.* **2022**, *6*, 24. [[CrossRef](#)]
16. Nicolodelli, G.; Tadini, A.M.; Nogueira, M.S.; Pratavieira, S.; Mounier, S.; Huaman, J.L.C.; dos Santos, C.H.; Montes, C.R.; Milori, D.M.B.P. Fluorescence Lifetime Evaluation of Whole Soils from the Amazon Rainforest. *Appl. Opt.* **2017**, *56*, 6936–6941. [[CrossRef](#)]
17. Tadini, A.M.; Nicolodelli, G.; Mounier, S.; Montes, C.R.; Milori, D.M.B.P. The Importance of Humic in Soil Characterisation: A Study on Amazonian Soils Using Different Fluorescence Techniques. *Sci. Total Environ.* **2015**, *537*, 152–158. [[CrossRef](#)]
18. Tadini, A.M.; Mounier, S.; Milori, D.M.B.P. Modeling the Quenching of Fluorescence from Organic Matter in Amazonian Soils. *Sci. Total Environ.* **2020**, *698*, 134067. [[CrossRef](#)]
19. Santos, C.H.; Nicolodelli, G.; Romano, R.A.; Tadini, A.M.; Villas-Boas, P.R.; Montes, C.R.; Mounier, S.; Milori, D.M.B.P. Structure of Humic Substances from Some Regions of the Amazon Assessed Coupling 3D Fluorescence Spectroscopy and CP/PARAFAC. *J. Braz. Chem. Soc.* **2015**, *26*, 1136–1142. [[CrossRef](#)]
20. Ishida, D.A.; Vieira-Coelho, A.C.; Melfi, A.J.; Lucas, Y.; Camargo, J.P.B.; Montes, C.R. Influence of Pedogenetic Processes on the Validity of Kaolinite Crystallinity Indices: A Case Study of an Amazonian Ferralsol-Podzol Soil System with White Kaolin. *Appl. Clay. Sci.* **2018**, *162*, 435–442. [[CrossRef](#)]
21. Nicolodelli, G.; Marangoni, B.S.; Cabral, J.S.; Villas-Boas, P.R.; Senesi, G.S.; dos Santos, C.H.; Romano, R.A.; Segnini, A.; Lucas, Y.; Montes, C.R.; et al. Quantification of Total Carbon in Soil Using Laser-Induced Breakdown Spectroscopy: A Method to Correct Interference Lines. *Appl. Opt.* **2014**, *53*, 2170–2176. [[CrossRef](#)]
22. Clabel, H.J.L.; Nicolodelli, G.; Senesi, G.S.; Montes, C.R.; Perruci, N.A.F.; Bezzon, V.D.N.; Balogh, D.T.; Milori, D.M.B.P. Organo-Mineral Associations in a Spodosol from Northern Brazil. *Geoderma Reg.* **2020**, *22*, e00303. [[CrossRef](#)]
23. Fang, F.; Min, F.; Liu, L.; Chen, J.; Ren, B.; Liu, C. Adsorption of Al(OH)(3+ (n = 2–4) on Kaolinite (001) Surfaces: A DFT Study. *Appl. Clay. Sci.* **2020**, *187*, 105455. [[CrossRef](#)]
24. Murad, E. Identification of Minor Amounts of Anatase in Kaolins by Raman Spectroscopy. *Am. Mineral.* **1997**, *82*, 203–206. [[CrossRef](#)]

25. Mineralogical Analysis by Infra-Red Spectrometry. In *Handbook of Soil Analysis*; Springer: Berlin/Heidelberg, Germany, 2006; pp. 133–165.
26. Kingma, K.J.; Hemley, R.J. Raman Spectroscopic Study of Microcrystalline Silica. *Am. Mineral.* **1994**, *79*, 269–273.
27. Michaelian, K.H. The Raman Spectrum of Kaolinite 9 at 21 °C. *Can. J. Chem.* **1986**, *64*, 285–294. [[CrossRef](#)]
28. Ruan, H.D.; Frost, R.L.; Kloprogge, J.T. Comparison of Raman Spectra in Characterizing Gibbsite, Bayerite, Diaspore and Boehmite. *J. Raman Spectrosc.* **2001**, *32*, 745–750. [[CrossRef](#)]
29. Milori, D.M.B.P.; Martin-Neto, L.; Bayer, C.; Mielniczuk, J.; Bagnato, V.S. Humification Degree of Soil Humic Acids Determined by Fluorescence Spectroscopy. *Soil Sci.* **2002**, *167*, 739–749. [[CrossRef](#)]
30. Tadini, A.M.; Nicolodelli, G.; Senesi, G.S.; Ishida, D.A.; Montes, C.R.; Lucas, Y.; Mounier, S.; Guimarães, F.E.G.; Milori, D.M.B.P. Soil Organic Matter in Podzol Horizons of the Amazon Region: Humification, Recalcitrance, and Dating. *Sci. Total Environ.* **2018**, *613–614*, 160–167. [[CrossRef](#)]

**Disclaimer/Publisher’s Note:** The statements, opinions and data contained in all publications are solely those of the individual author(s) and contributor(s) and not of MDPI and/or the editor(s). MDPI and/or the editor(s) disclaim responsibility for any injury to people or property resulting from any ideas, methods, instructions or products referred to in the content.